Tectonics®

RESEARCH ARTICLE
10.1029/2021TC007115

Key Points:

- We carried out a detailed structural analysis of the Afrera Plain linkage zone using 1 m Digital Elevation Models obtained from tri-stereo Pléiades-1 imagery
- Dikes and faults are coeval and both accommodate strain in the linkage zone
- Diking accommodates pure extension, while conjugate faults accommodate both shear and extension during rift–rift interaction

Supporting Information:

Supporting Information may be found in the online version of this article.

Correspondence to:

A. La Rosa,
alessandro.larosa@dst.unipi.it

Citation:

La Rosa, A., Pagli, C., Hurman, G. L., & Keir, D. (2022). Strain accommodation by intrusion and faulting in a rift linkage zone: Evidences from high-resolution topography data of the Afrera Plain (Afar, East Africa). *Tectonics*, *41*, e2021TC007115. https://doi.org/10.1029/2021TC007115

Received 22 OCT 2021
Accepted 18 MAY 2022

Strain Accommodation by Intrusion and Faulting in a Rift Linkage Zone: Evidences From High-Resolution Topography Data of the Afrera Plain (Afar, East Africa)

Alessandro La Rosa[1], Carolina Pagli[1], Gareth L. Hurman[2], and Derek Keir[2,3]

[1]Dipartimento di Scienze della Terra, Università di Pisa, Pisa, Italy, [2]School of Ocean and Earth Science, University of Southampton, Southampton, UK, [3]Dipartimento di Scienze della Terra, Università degli Studi di Firenze, Firenze, Italy

Abstract At mature magma-rich continental rifts, extension focuses along discrete axial segments where magmatism and diking are important in accommodating plate divergence. However, the role of magma in influencing the deformation at rift–rift offsets is still unclear as direct observations are rare. Here, we exploited high-resolution Pléiades-1 tri-stereo imagery to produce the first 1 m Digital Elevation Model of the Afrera Plain linkage zone between the Erta Ale and Tat Ali magmatic segments in Northern Afar. We carried out a detailed structural analysis of both tectonic and magmatic features in the area and observed different trends and kinematics of these features. Magmatic features at Afrera strike N160°E ± 5°E, similar to the Erta Ale segment and perpendicular to the extension direction. Conversely, tectonic features fall into two families of ~NW-SE- and ~NS-striking oblique faults with right-lateral and left-lateral components, respectively, as shown by Riedel shears. We interpret the extension direction of tectonic features using observed opening of fractures, previous seismic, and InSAR-based fault models and from that expected for the mapped conjugate fault pattern. While the results show scatter in the range of N46°E–N68°E, it is similar within error to the regional extension direction. The simplest model that explains our data is that in the linkage zone there is both extensional and shear strain. The dikes accommodate only extension, while conjugate oblique faults accommodate extension and shear strain. Our study shows that both magmatism and faulting are important during rift segment interaction and linkage.

Plain Language Summary When two tectonic plates separate, the lithosphere extends through the intrusion of molten rock (magma) rising from depth and with brittle faulting occurring in the upper crust. As extension proceeds, the magma emplacement focuses in ~50–100-km-long, and tens-of-kilometers-wide linear segments (magmatic segment) of the rift valley floor, with a sideways step (lateral offset) commonly present in-between adjacent segments. However, the style of faulting and the role of magmatic activity in influencing the deformation in the lateral offsets between magmatic segments are not well understood. In this study, we addressed this open question by creating high-resolution combined three-tridimensional models of the Earth surface and interpreting it with high-resolution satellite images. We map fractures and other structures related to magmatic activity and collect measurements showing that two different types of coexisting deformation can be accommodated by either magmatic and or nonmagmatic processes.

1. Introduction

In mature magma-rich continental rifts, plate divergence mainly occurs in a narrow zone of the rift valley floor as a series of discrete magmatic segments where magmatism and faulting are the main mechanisms to accommodate the lithospheric extension (Buck, 2006; Hayward & Ebinger, 1996; Keir et al., 2009; Rowland et al., 2007). Extension in the magmatic segments commonly manifests through recurrent single dike intrusions (e.g., Moore et al., 2019; Nobile et al., 2012; Xu et al., 2017) and also through major diking episodes in which cubic kilometers of magma are emplaced in tens-of-kilometers-long crustal portions (e.g., Einarsson & Brandsdóttir, 1980; Grandin et al., 2010; Sigmundsson et al., 2015; Wright et al., 2012). Such major events occur within ~10^2- to 10^3-year-long cycles, including codiking, postdiking, and interdiking phases (Pagli et al., 2015; Wright et al., 2012).

As extension proceeds, adjacent magmatic segments interact through linkage zones that are thought to potentially evolve to form oceanic transform faults once continental breakup occurs (Brune et al., 2017; Corti, 2012; Doubre et al., 2017; Illsley-Kemp et al., 2018; Le Pourhiet et al., 2017; Manighetti et al., 2001; Pagli et al., 2019). However, the kinematics of faulting and rift–rift interaction, along with the magmatism in linkage zones, is

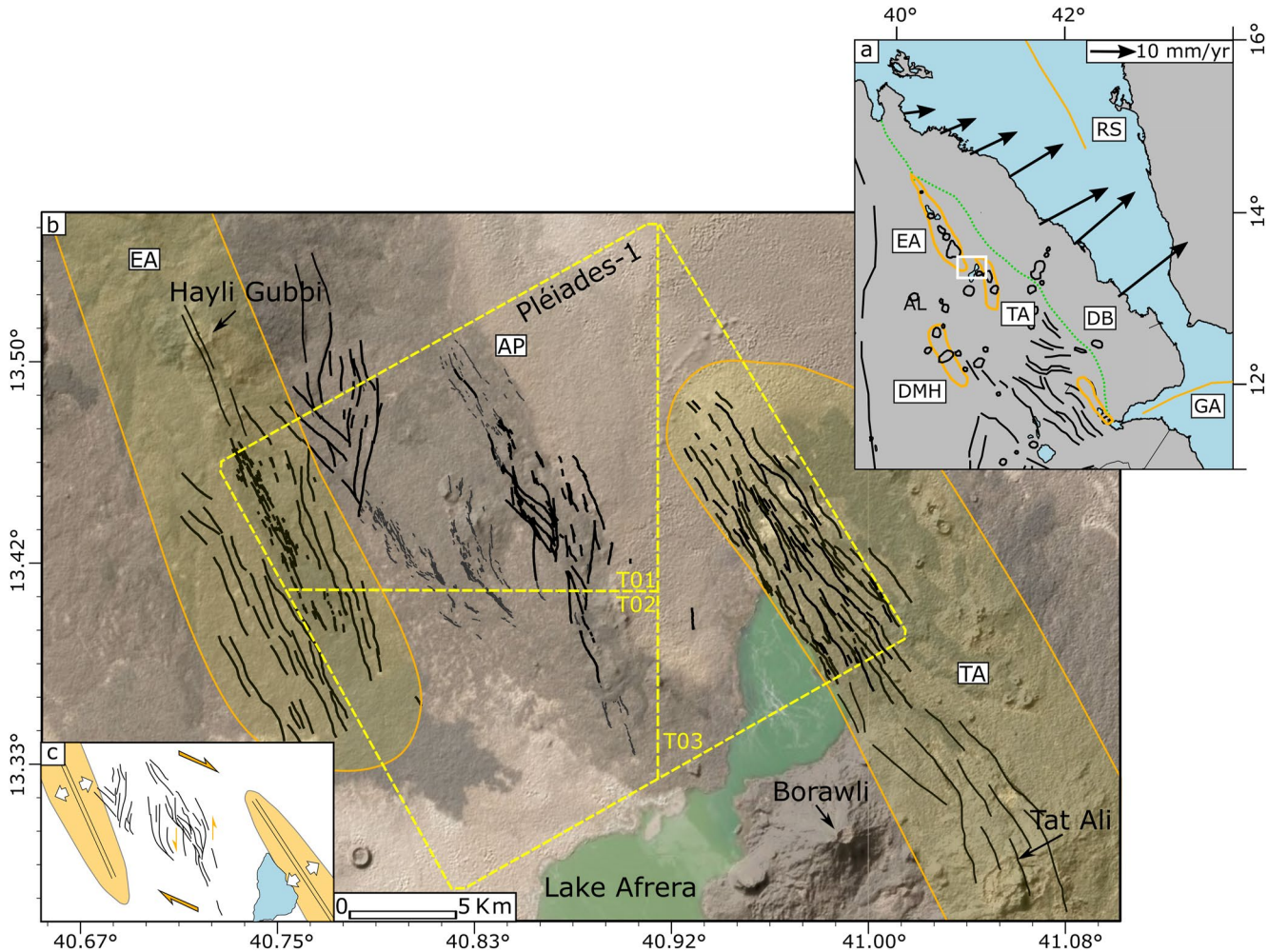

Figure 1. Tectonic setting of Afar and main structures of the Afrera Plain. (a) Afar region with major faults (black lines) and magmatic segments (orange polygons): EA, Erta Ale segment; TA, Tat Ali segment; AP, Afrera Plain; DMH, Dabbahu–Manda-Harraro segment. RS is the Red Sea rift; GA is the Gulf of Aden rift. GPS horizontal velocities (black arrows) with respect to stable Nubia are from Viltres et al. (2020). The green line marks the Danakil Block (DB). The white box marks the study area in (b) where black lines are structures (modified from La Rosa et al., 2019) and the yellow dashed polygons show the area covered by three Pléiades-1 triplets used in this study. (c) Sketch of the kinematic model proposed for the Afrera Plain by La Rosa et al. (2019).

debated, as is how tectonic and magmatism interact in space and time. Previous studies have documented the occurrence of magmatism at linkage zones not only along the East African Rift, such as in Central Afar, in the Kivu–Rusizi rift, and the Rungwe Volcanic Province (Acocella, 2010; Ebinger, 1989; Ebinger et al., 1989), in the Basin and Range province (Faulds & Varga, 1998), but also along the Mid-Atlantic Ridge (Koopmann et al., 2014). It was proposed that the presence of magma may favor the propagation and linkage of two graben-like structures (Faulds & Varga, 1998). Alternatively, numerical models by Koopmann et al. (2014) showed that a delay in the onset of extension may promote mantle decompression between two rift segments and the generation of magma at the linkage zone. Analog models by Corti et al. (2002, 2004) instead suggested a mutual relationship between magmatism and tectonics at linkage zones with magma controlling the distribution of deformation and faulting influencing the pathways of magma migration to shallow crustal levels.

In this study, we focused on the Afrera Plain, the offset between the two active magmatic segments of Erta Ale and Tat Ali, in Northern Afar (Figure 1). Previous studies combined structural data with InSAR and seismicity observations to show that the Afrera Plain is a right-lateral linkage zone accommodating deformation mainly through a system of NS-striking, oblique left-lateral faults (Figure 1c; La Rosa et al., 2019, 2021). The existence of a minor conjugate population of oblique right-lateral faults was also inferred on the basis of previous seismicity observations (Illsley-Kemp et al., 2018; La Rosa et al., 2019). InSAR time-series showed that faults at the Afrera

Plain have varying fault behavior encompassing stick-slip with $M_w \geq 5$ earthquakes and creep accompanied by minor seismicity (La Rosa et al., 2021). Such behaviors were interpreted as influenced by the presence of magma and hydrothermal fluids below the Afrera Plain (La Rosa et al., 2021). Magmatic activity in the area is also suggested by the presence of eruptive fissures and recent lava flows close to active faults. However, how strain is accommodated by intrusions and by faulting remains poorly investigated.

Here, we address this question by carrying out detailed mapping of the tectonics and magmatic structures of the Afrera Plain using very high-resolution Pléiades-1 satellite imagery. We combined tri-stereo panchromatic Pléiades-1 images of the Afrera Plain to produce a high-resolution (1 m) Digital Elevation Model (DEM) of the study area. The data set enabled us to map tectonic and magmatic structures of the Afrera Plain to an unprecedented level of detail and to apply quantitative analyses to our results. For the first time, we were able to solve for geometry, throws, and kinematics of faults and fractures across the study area. We also measured opening directions across tectonic fractures and dike-related extension directions to understand whether and how the strain field varied. We find that the strain is accommodated by intrusions with a ∼N65°E extension direction and by conjugate oblique faulting with extension varying between N46°E and N68°E. We favor the interpretation that the scatter in fault recorded extension is due to natural variability and that dikes and faults form in the same strain field. In this scenario, the dikes take up extension and the oblique slip faults take up extension and the shear strain consequent of rift segment link. We also discuss the implications of interpreting the rotation of strain through time.

2. Geological and Tectonic Setting

Since ∼30 Ma, the Red Sea, the Gulf of Aden, and the Main Ethiopian rifts have been accommodating the plate divergence of Nubia, Arabia, and Somalia (Figure 1a). These three rift arms meet today in the Afar depression to form a rift–rift–rift triple junction (Barberi & Varet, 1970; Beyene & Abdelsalam, 2005; Manighetti et al., 1998). During the last 11 Ma, the southward propagation of the Red Sea rift in Northern Afar led to the separation of the Danakil Block and the rotational opening of the Danakil Depression (e.g., Eagles et al., 2002; McClusky et al., 2010; Zwaan et al., 2020). Starting from the Quaternary, plate divergence in Afar is mainly accommodated along a series of en echelon magmatic segments where extension occurs through dominant magmatic activity characterized by diking episodes, volcanic eruptions, and minor faulting in the upper crust (Barnie et al., 2016; Buck, 2006; Hayward & Ebinger, 1996; Rowland et al., 2007; Tortelli et al., 2021). The axial zone of magmatic segments along the Danakil Depression mostly defines an axial high topography (e.g., Pagli et al., 2012). The magmatic segments are bounded on both sides by conjugate systems of normal faults getting younger near the segment axis and develop a graben-like structure similar to those observed at slow-spreading mid-ocean ridges (Barberi & Varet, 1970).

Horizontal GPS velocities measured in Northern Afar during 2001–2016 show that the ongoing separation of the Danakil Block has a mean direction of ∼N60°E, with velocities progressively increasing southward, from ∼10 mm/year at latitude N14.5° to ∼16 mm/year at latitude N12.7° (McClusky et al., 2010; Viltres et al., 2020). In Northern Afar, the opening of the Danakil Depression is accommodated by two main axial magmatic segments: the Erta Ale and the Tat Ali. The Erta Ale segment is ∼125-km long and strikes in a NNW-SSE direction, from the Dallol salt plain, at latitude ∼N14.3°, to the Afrera Plain, at latitude ∼N13.3° (Barberi & Varet, 1970). The segment is characterized by a series of axial volcanic centers whose shallow, <3 km depth, magma chambers fed the recent diking events at Dallol and Erta Ale in 2004 (Barnie et al., 2016; Battaglia et al., 2021; Nobile et al., 2012) as also the last eruptions at Alu-Dalafilla and Erta Ale of 2008 and 2017, respectively (Battaglia et al., 2021; Moore et al., 2019; Pagli et al., 2012; Xu et al., 2017). Besides these recent episodes, the lava flow record shows that fissural eruptions have previously occurred along fractures and vents near the axis of the magmatic segments (Acocella, 2006; Barberi & Varet, 1970; Watts et al., 2020).

The Tat Ali segment is left-stepped with respect to the Erta Ale segment, it extends for ∼60 km, and hosts the main Tat Ali volcano (Figure 1). Similar to the Erta Ale, the Tat Ali segment shows normal faults, axial volcanoes, and eruptive fissures (Barberi & Varet, 1970). Unlike the Erta Ale segment, the trend of the Tat Ali segment changes from NW-SE north of the Tat Ali volcano to NNW-SSE south of it, resulting in an arcuate shape of the segment (Figure 1a). Furthermore, south of ∼N13.1°, the faults split into two main families trending NS and NE-SW, respectively (e.g., Barberi & Varet, 1977; Schaegis et al., 2021). The latter trend has been proposed to be

associated with a left-lateral linkage zone developing south of the Afdera volcano and transferring the displacements from the Tat Ali segment to the right-stepped Dabbahu–Manda-Hararo segment to the south (Figure 1a; Barberi & Varet, 1977; Muluneh et al., 2013; Schaegis et al., 2021).

The Afrera Plain is a ∼20-km-wide zone where the Erta Ale and Tat Ali segments overlap. This area hosts an hypersaline lake fed by hydrothermal springs, known as Lake Afrera (Bonatti et al., 2017). The whole area is below sea level (b.s.l.), with the lowest elevation of ∼190 b.s.l. recently measured at the lake floor (Schaegis et al., 2021). To the west, Lake Afrera is bounded by a salt plain hosting evaporitic, lacustrine, and marine deposits (0.006–0.025 Ma; Barberi & Varet, 1970; Barberi et al., 1972). North and east of the lake, Quaternary (<1.2 Ma) basalts and picritic basalts resulting from subaerial eruptions are also observed (Barberi & Varet, 1970, 1972). To the north, the basalts are dissected by systems of fractures and oblique faults accommodating the right-lateral shear between the two magmatic segments (Illsley-Kemp et al., 2018; La Rosa et al., 2019), while the eastern lake's shore is controlled by a system of W-dipping normal faults (Bonatti et al., 2017).

Recent InSAR and seismicity at the Afrera Plain provided a picture of the ongoing strain showing that NS-striking faults with oblique left-lateral slip accommodate most of the right-lateral shear (Figure 1c), while a conjugate fault system of NW-SE-striking oblique, right-lateral faults was also inferred from seismic observations (Illsley-Kemp et al., 2018; La Rosa et al., 2019). Recently, echo-sounding measurements below Lake Afrera by Schaegis et al. (2021) also showed the presence of systems of NS- and NW-striking faults, similar to those observed to the north.

3. Methods

We produced a high-resolution topography data set of the Afrera Plain by applying photogrammetry techniques on tri-stereo satellite imagery. The data set has been then used to map manually tectonic and magmatic structures in the study area and carry out an analysis of their geometry and kinematic indicators.

3.1. DEM Processing

In 2020, we tasked acquisitions of panchromatic (0.5 m resolution) and multispectral (2 m resolution) imagery by the Pléiades-1 satellites of an area encompassing the Afrera Plain and its connection to the Erta Ale and Tat Ali segments. The Pléiades-1 satellites made three separate adjacent acquisitions to cover the area, between August and September 2020 (Figure 1b). All the acquisitions were obtained under excellent weather conditions (100% cloud free) and in tri-stereo allowing for three quasi-simultaneous images (triplet) of the same area from three different incidence angles: a forward-looking (FL, average incidence angle 6.2°), a quasi-nadir (QN, incidence angle 1.6°), and a backward-looking (BL, incidence angle −6.3°) image (Gleyzes et al., 2012). Each triplet was combined through photogrammetric processing to derive three 1 m resolution DEMs.

We used the Geomatica Banff OrthoEngine software (PCI Geomatics, e.g., Toutin & Cheng, 2002) to derive the DEMs from the panchromatic Pléiades-1 triplets (here referred to as T01, T02, and T03; Figure 1b). The alignment of the triplets is a key step in the DEM extraction as precise image overlap is necessary to obtain accurate tridimensional information of the Earth surface. For this step, we used tie points (TPs)—the same feature identifiable in the different images. We identified a total of 411 TPs over the whole study area: 92 TPs in T01, 101 TPs in T02, and 218 TPs in T03. The horizontal shift between images calculated at the TPs has an average root mean square misfit of <0.09 pixels for T01 (∼0.05 m), <0.1 pixels for T02, and 0.2 pixels for T03 (Text S1 in Supporting Information S2).

We generated three DEMs (Data Set S1) for each triplet using the image pairs FL–QN, QN–BL, and FL–BL. The three DEMs were processed with a sampling interval of 0.5 m and then stitched together to extract a final DEM with resolution of 1 m. The residual artifacts (bumps and pits) affecting the areas covered by sands were filtered out manually through a series of cascade spatial filters with progressively decreasing window size (from 23 to 7 pixels) and gradient (from 15° to 5°; Figures S1a and S1b in Supporting Information S1). As a last step, the Afrera Lake was masked as artifacts occurred over the water surface (Figures S1c and S1d in Supporting Information S1). Finally, the three original QN panchromatic images were orthorectified and used together with the derived DEMs to map the structures of Afrera Plain.

3.2. DEM Analysis

We manually mapped tectonic and magmatic features with ArcGis Pro. The majority of the mapping was carried out using the novel Pléiades-1 data set, but we completed the mapping on the parts of the segments that were not imaged by Pléiades-1 (Figure 1b) using the 1 arc-sec (30 m) Shuttle Radar Topography Mission (SRTM) DEM (Farr et al., 2007) and the SPOT (From French: Satellite pour l' Observation de la Terre) Imagery (2.5 m). We use this low-resolution data set just to map faults with clear scarps and other features that were partially covered by the Pléiades-1 data set. We used the Pléiades-1 DEMs to calculate maps of the slope and topographic profiles for mapping structures. Then, we used DEMs together with panchromatic images to record the morphology, geometry, and vertical displacement (throw) of the structures (e.g., Bubeck et al., 2018; Tibaldi et al., 2020; Wilson et al., 2007). We divided our study area into three main domains: the southern Erta Ale segment, the northern Tat Ali segment, and the Afrera Plain (Figure 1b) as previously done by La Rosa et al. (2019). For all the structures, we produced length-weighted rose diagrams of the strikes (measured tip-to-tip) to solve for the dominant trends in the different domains.

Faults were mapped on the basis of the presence of a topographic scarp highlighted by the slope layer. Faults were also inferred where monoclines and Riedel structures at the surface indicated the presence of a buried fault (e.g., Bubeck et al., 2018; Dooley & Schreurs, 2012; Holland et al., 2006). Fault scarps were grouped into W-SW-dipping and E-NE-dipping. Buried faults were mapped separately as we could not constrain their dip.

Secondary faults can develop not only at the tips but also at the footwalls and hanging-walls of major faults and they may be differently oriented due to local perturbation of the regional stress field during the growth of the major faults along which they form (e.g., Holland et al., 2006; Kim et al., 2004). Therefore, we mapped secondary faults separately.

Linear structures that were visible in the panchromatic images but lack a measurable throw in our DEMs were classified as fractures. We excluded from our mapping fractures at the footwalls of fault scarps, as they could be caused by gravitational motions rather than by tectonics (Tibaldi et al., 2020). We assumed fractures to be caused by horizontal displacements (extension, shear, or mixed mode), yet we cannot exclude that some of the fractures have some vertical displacement, not measurable at the resolution of our DEMs.

Regarding the mapping of magmatic features, we looked for distinctive structures at the surface that indicate dike intrusion in the shallow crust. In particular, dikes propagating through the crust are known to generate graben-like structures with a depressed axial region bounded by normal faults and uplifted flanks (e.g., Grandin et al., 2010; Holland et al., 2006; Trippanera, Acocella, et al., 2015; Trippanera, Ruch, et al., 2015). When a dike reaches the surface forming an eruptive fissure, lava flows and often alignments of vents occur. We thus mapped alignments of vents and fractures with lava flows as eruptive fissures. Furthermore, faults and fractures spatially associated with volcanic structures, for example, vents forming along faults, or fractures forming along eruptive fissures, were classified as dike induced.

In summary, we created six classes for the tectonic structures: E-NE-dipping faults, E-NE-dipping secondary faults, W-SW-dipping faults, W-SW-dipping secondary faults, faults with no dip, and fractures. Magmatic structures were instead grouped in three classes: eruptive fissures, dike-induced faults, and dike-induced fractures.

We finally investigated the kinematics of the tectonic structures in the Afrera Plain by collecting kinematic indicators across both faults and fractures. For the faults, we analyzed patterns of secondary features, such as shallow splays, fracture systems, and monoclines, to determine the sense of slip and the direction of propagation of the fault rupture. For fractures, we measured the opening directions using the Pléiades-1 orthoimages by matching pairs of asperities on both sides of fractures (Acocella et al., 2000). This method is widely used in the field (e.g., Acocella & Korme, 2002; Bubeck et al., 2017; Gudmundsson, 2003; Tentler, 2005; Tibaldi et al., 2016) but recent studies showed that it can be successfully applied on high-resolution satellite and airborne imagery (e.g., Tibaldi et al., 2020; Trippanera, Ruch, et al., 2015; Trippanera et al., 2019). Following similar previous works (Acocella et al., 2000; Tibaldi et al., 2020; Trippanera et al., 2019), we took a series of precautions to avoid misleading observations. In particular, we measured opening directions in flat areas far from the fault scarps to avoid any effect of local gravitational motions, and we avoided measurements at the fractures tips as rotations can occur between interacting fractures (Tibaldi et al., 2020). When possible, we made multiple measurements along the same fracture to get statistically meaningful values, and we avoided funnel-shaped fractures as this morphology

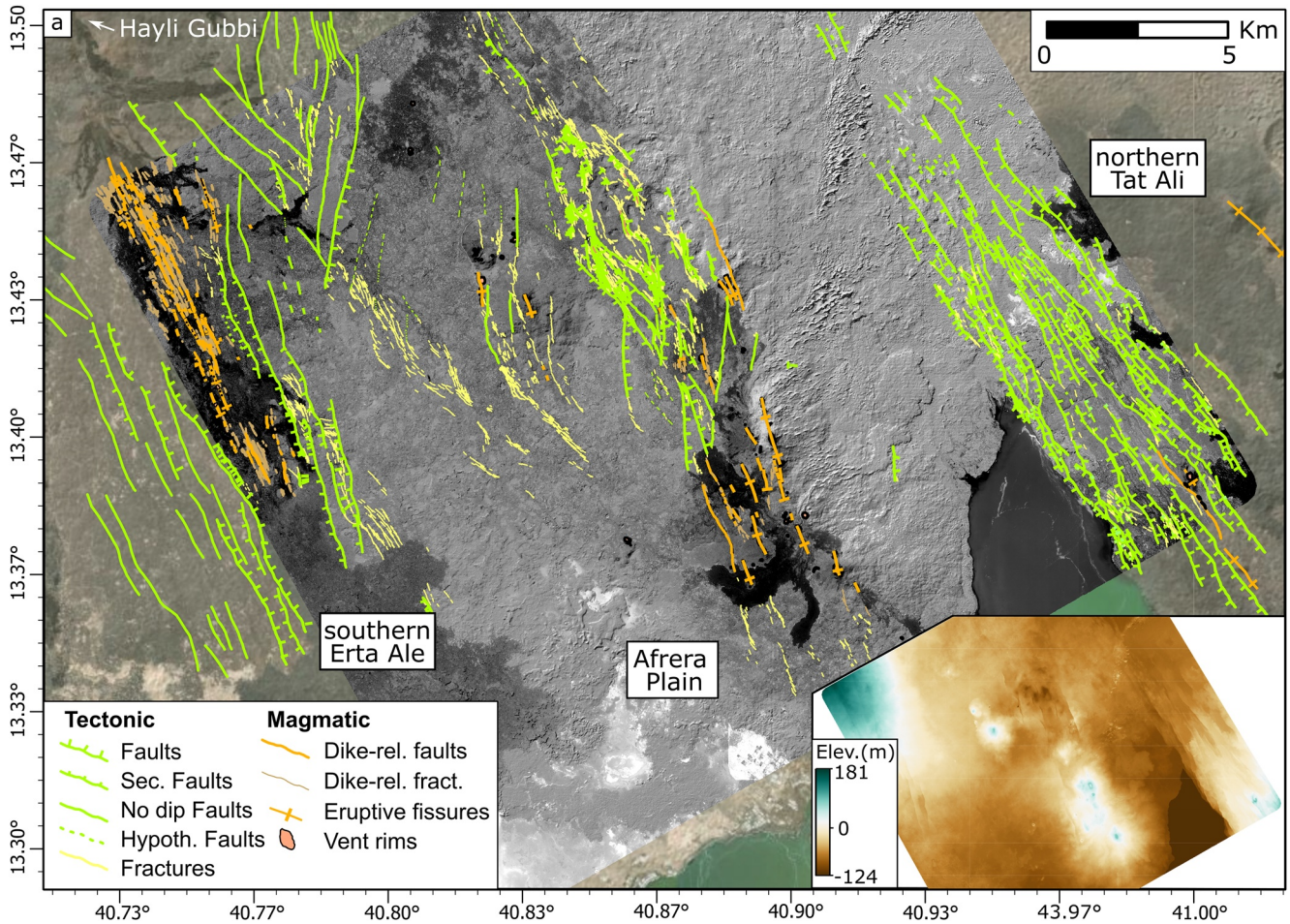

Figure 2. Full structural map of the southern Erta Ale segment, the northern Tat Ali, and the Afrera Plain. The area in grayscale is that covered by Pléiades-1, with the panchromatic image draped on the Pléiades-1 Digital Elevation Model (DEM). The color area outside is covered just by the ancillary low-resolution data set with the SPOT multispectral imagery available in ArcGis PRO draped on the SRTM 30 m DEM. The inset shows the topography of the study area obtained from the Pléiades-1 DEM. A detailed view of the three separated domains can be found in Figures 3–5.

could result from collapses of the fracture walls (Tibaldi et al., 2020). Finally, we checked the reliability of our of satellite imagery mapping by comparing remotely collected measurements to those collected in the field (La Rosa et al., 2019).

4. Results

Using our high-resolution Pléiades-1 data set, we mapped 8,278 tectonic and magmatic features within the southern Erta Ale segment, the northern Tat Ali segment, and Afrera Plain (Figure 2). Here, we will present the results of the structural mapping by describing quantitative and qualitative observations for these three areas separately. In the following analysis, we report the 95% confidence interval for each average strike we calculated throughout the study area.

4.1. Southern Erta Ale

A total of 2,511 tectonic and magmatic features were mapped at the southern tip of the Erta Ale segment (Figure 3). Magmatic features are mainly focused on a 2–4-km-wide axial region where dike-fed eruptive fissures and lava flows mark the locus of the recent-most magmatic activity. These features occur over a progressively wider area moving northward, toward the Hayli Gubbi volcano. The major eruptive fissures have a length between ~0.5 and ~1.5 km with vents aligned along the axis and in some cases hosted within narrow, 10–40-m-wide, grabens

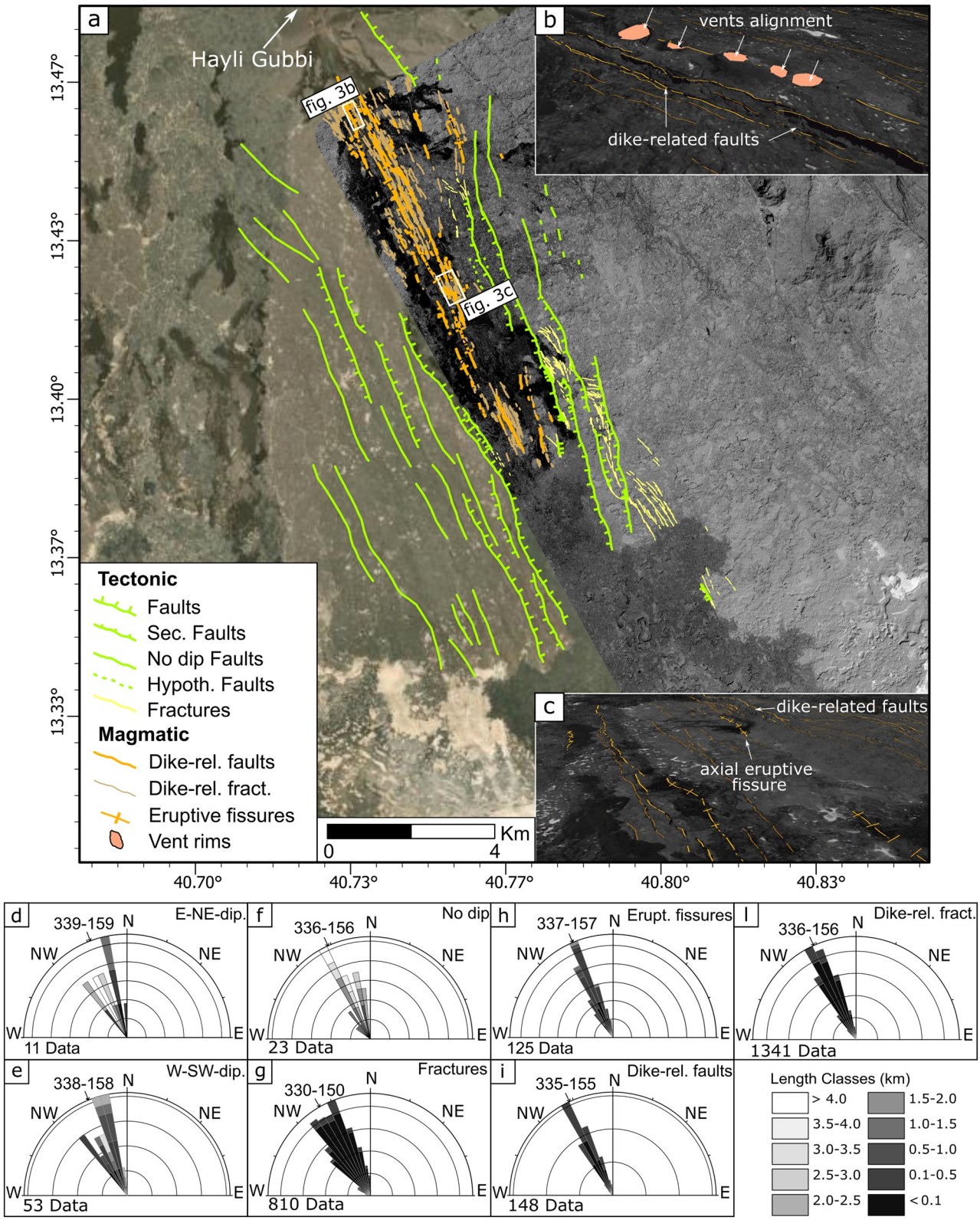

Figure 3.

(Figures 3b and 3h–3l Figures S2 and S3 in Supporting Information S1). Larger grabens (>200-m-wide) are found where recent lava flows are observed flowing out from fractures at both graben axis and flanks (Figure 3c and Figure S3b in Supporting Information S1). Overall, long eruptive fissures with vents alignments are just a small percentage of the whole population. Instead, ~92% of the eruptive fissures originate from short separate (<0.5 km) fractures. Irrespective of the varying length and morphology of magmatic structures, all of them show a similar strike of N157°E ± 3°E.

Tectonic features bound the axial portion of the Erta Ale segment on both sides with normal faults having lengths >4 km and maximum throws of ~15 m. Faults have dips of 65°–85° southwestward directed on the eastern side and northeastward directed on the western side of the Erta Ale segment. All faults show a consistent N157°E ± 3°E strike, very similar to the magmatic structures on the axis (Figure 3).

4.2. Northern Tat Ali

At the north-western portion of the Tat Ali segment, we mapped 719 tectonic and magmatic features (Figure 4). Tectonic features are dominant with 717 faults and fractures, while we observed magmatic features only in the southern portion of the study area. Magmatic features consist of a series of vents aligned in a N145°E direction and cut by a SW-dipping normal fault. Few major eruptive fissures were also mapped outside the Pléiades-1 data set using the lower resolution data set. We point out that our observation of dominant tectonic features is restricted to the area covered by the Pléiades-1 data set as vent alignments and fresh lava flows are also observed east and south of this area (Figures 4a and 4b). Yet the resolution of the ancillary data set does not allow for a complete mapping.

In the area covered by Pléiades-1, tectonic features show a homogenous distribution and orientation with 2–4-km-long normal faults striking ~N147°E ± 3°E (Figures 4c–4e). The interplay between SW- and NE-dipping faults creates hundreds-of-meters-large grabens hosting secondary faults, recent sediments, and lava flows (Figures 4a and 4b).

Part of the recent sediments are associated with ephemeral river networks that are observed flowing northwestward and following the regional decrease in elevation along the major axis of the magmatic segment (Figures S2 and S4a in Supporting Information S1). The sedimentary processes also occur at the northern termination of the Tat Ali segment where eolian sediments and dunes cover almost all the basaltic bedrock (Figure 4a).

Several generations of lavas are also observed flowing northwestward and partially filling the tectonic grabens (Figure 4a and Figure S4a in Supporting Information S1). A structural control over the direction of lavas is evident where the fault scarps act as a barrier for the flows, favoring the formation of lava channels (Figures 4a and 4b; Figure S4a in Supporting Information S1). Here, fractures within the lavas striking parallel to major faults are observed to form due to differential flows between the internal hot and the external cooler portions of the same lava flow (Figure 4b and Figure S4a in Supporting Information S1; e.g., Calvari, 2019; Cashman et al., 2013; Wentworth, 1954). The channels are also locally characterized by levée structures forming right above fault-controlled topographic highs (Figure S4b in Supporting Information S1). Where lavas overcame the fault scarps, the flows bifurcated and moved west-southwestward following a secondary decrease in elevation controlled by the fault motions (Figure 4b and Figure S4c in Supporting Information S1).

The above-mentioned erosional, sedimentary, and volcanic processes modify the original fault morphology at the surface, preventing an accurate estimation of the faults' dip angles and throws in most of the area. However, where the fault scarps are neither eroded nor partially covered, they are steep (~75°) and reach throws of ~30 m. While the two fault families have comparable lengths (Figures 4c and 4d), the highest throws were measured along SW-dipping faults with maximum values observed along the shores of the Afrera Lake where such structures mark the strongest decrease in elevation and control the evolution of the eastern shore of the lake.

Figure 3. Structural map and statistical analysis of the southern Erta Ale segment. (a) Map showing the tectonic and magmatic features identified in the area. The area in grayscale is that covered by Pléiades-1, with the panchromatic image draped on the Pléiades-1 Digital Elevation Model (DEM). The color area outside is covered just by the ancillary low-resolution data set with the SPOT multispectral imagery available in ArcGis PRO draped on the SRTM 30 m DEM. (b, c) Details of magmatic features in the southern Erta Ale. (d–l) Length-weighted rose diagrams of the mapped structures. The binning is 5° and the number reported on each diagram is the average strike.

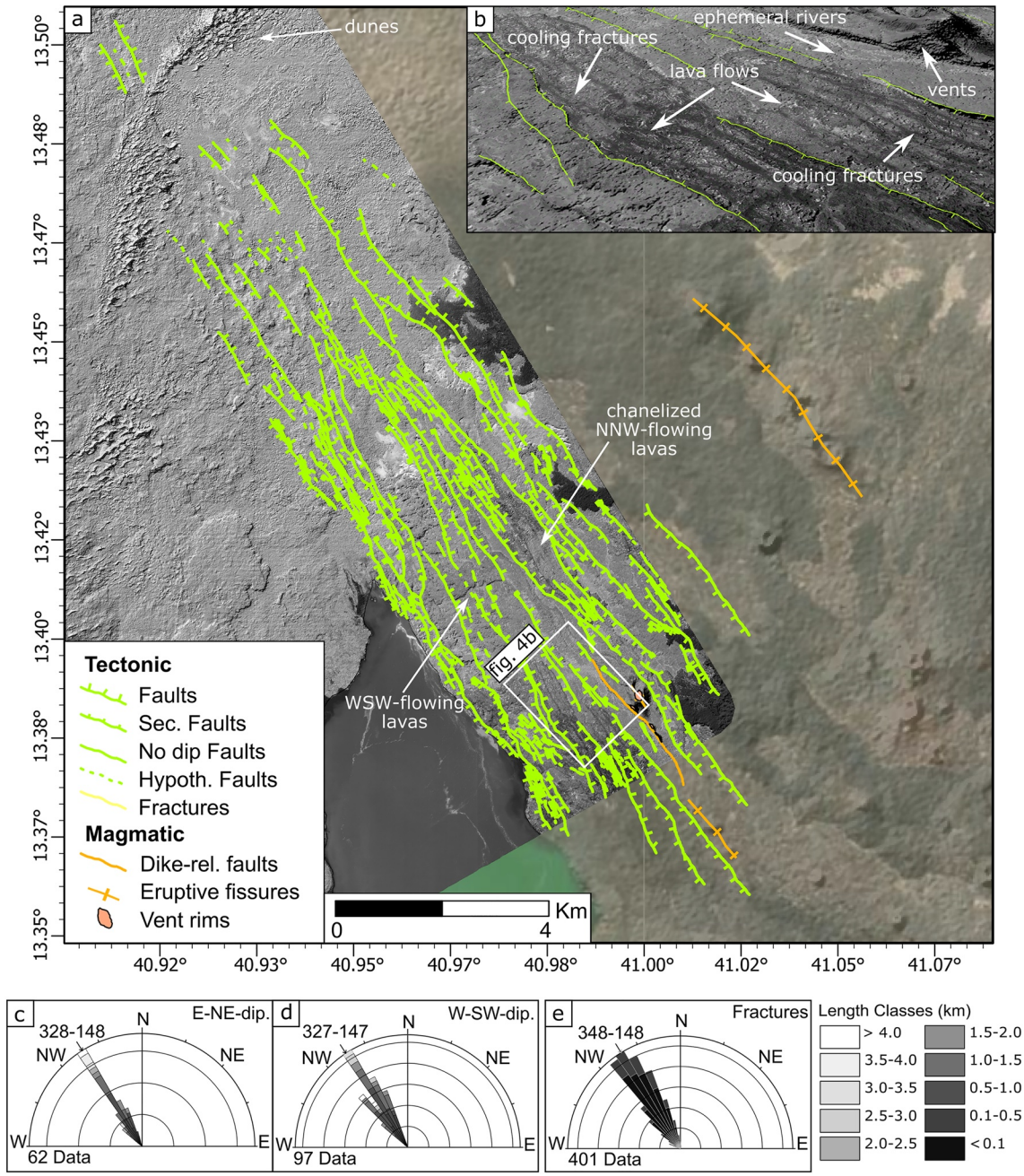

Figure 4. Structural map and statistical analysis of the northern Tat Ali segment. (a) Map showing the tectonic and magmatic features identified in the area. As in Figure 3, the area in grayscale is that covered by Pléiades-1, with the panchromatic image draped on the Pléiades-1 Digital Elevation Model (DEM). The color area outside is covered just by the ancillary low-resolution data set with the SPOT multispectral imagery available in ArcGis PRO draped on the SRTM 30 m DEM. (b) Details of the magmatic features and relationship between lavas and faults. (c–e) Length-weighted rose diagrams of tectonic features. The binning is 5° and the number reported on each diagram is the average strike.

4.3. The Afrera Plain

Mapping at the Afrera Plain revealed the presence of 4,915 tectonic and magmatic features (Figure 5a). These features are not homogenously distributed over the Afrera Plain yet zones of intense faulting, fracturing, and magmatism can be observed to be separated by areas with minor deformation. A striking characteristic is the presence of a main system of faults, fractures, and dike-related structures between longitudes E40.82° and E40.92°, where ~70% of the features mapped in the Afrera Plain are present.

10.1029/2021TC007115

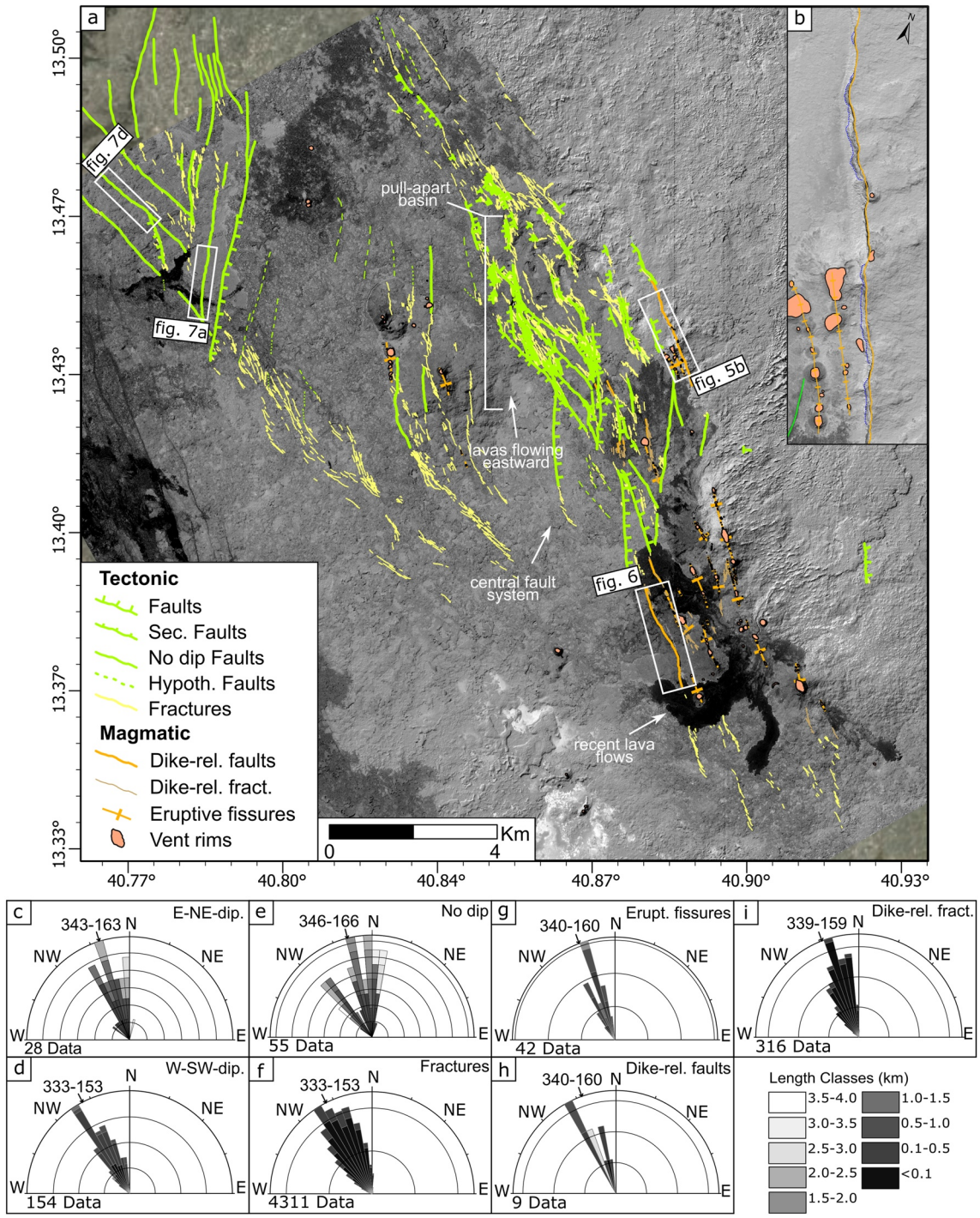

Figure 5. Structural map and statistical analysis of the Afrera Plain. (a) Map showing the tectonic and magmatic features identified in the area. (b) Details of magmatic features observed in the northern part of the Afrera Plain. (c–i) Length-weighted rose diagrams of tectonic features. The binning is 5° and the number reported on each diagram is the average strike.

Magmatic activity in the Afrera Plain is observed in three main distinct areas. The first area is located at latitudes between N13.34°–N13.41° where a volcanic field covering a ~32-km^2-wide area shows dark lava flows (Figure 5a). Here, lava flows are fed from eruptive fissures striking in a N160°E ± 5°E direction (Figures 5a and 5g–5i), similar to the trend measured at the southern Erta Ale segment. Most of the eruptive fissures are located within a half-graben, bounded to the west by an east-dipping normal fault (Figures 5 and 6). At the

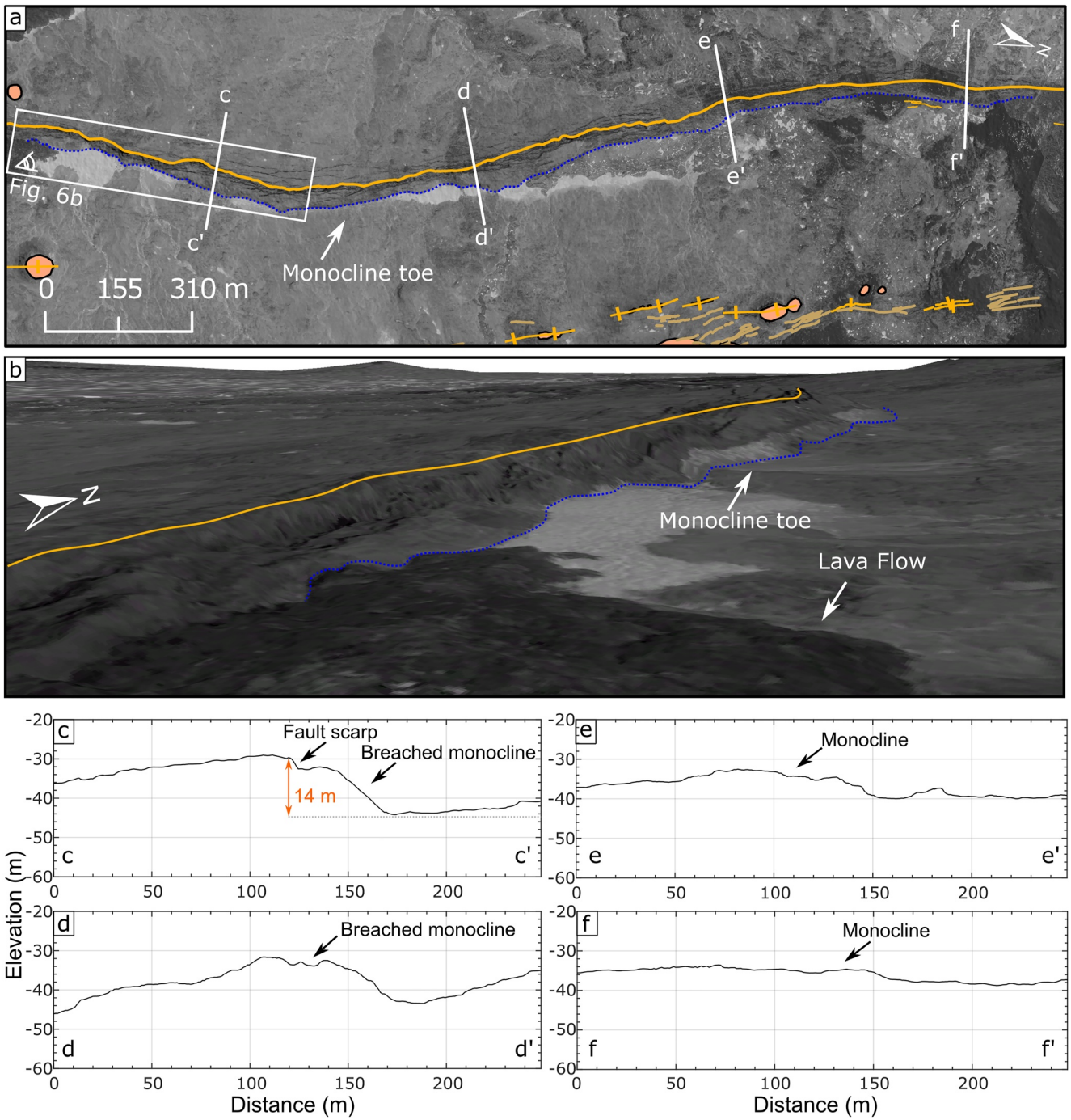

Figure 6. Map view, tridimensional view, and cross sections of a dike-related fault at the Afrera Plain see Figure 5 and Figure S2 in Supporting Information S1 for location. (a, b) The figures show an E-dipping dike-related fault characterized by a continuous monocline structure and several eruptive fissures along the hanging-wall. Note some dark lava flowing out of fractures close to the fault scarp in the northern sector. In (b), the fault can also be seen to act as a barrier for another lava flow. The view direction is reported in the white box in (a). (c–f) Cross section showing the along-fault variations of throws and morphology. Local breaches in the monocline highlight a fault throw (orange arrow) of 14 m in (c).

surface, this fault is characterized by a continuous monocline structure (Figure 6). Local breaches in the monocline highlight a topographic scarp with dip angle of ~50° and throws of ~14 m (Figure 6b). The second area is located further to the north, where a NNW-striking, WSW-dipping fault scarp, with throws >30 m, dissects a series of vents and generates a half-graben structure hosting eruptive fissures that strike in the same NNW

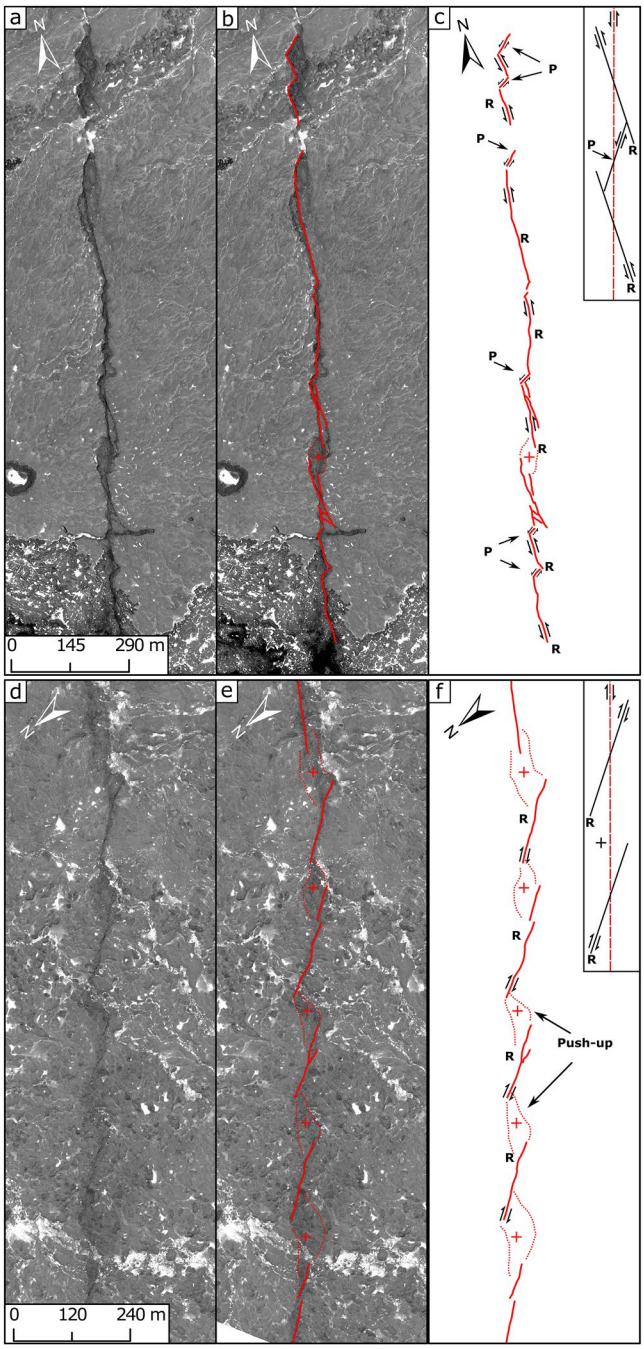

Figure 7. Conjugate faults in the Afrera Plain showing Riedel shears with opposite sense of motion. (a–c) ~NS-striking fault with R and P shears indicating a left-lateral kinematics. (d–f) NW-striking fault at the interaction between Erta Ale segment and Afrera Plain with R shears indicating a right-lateral kinematics. The insets in (c) and (f) show a schematic reprisal of Riedel shears (modified from Dooley & Schreurs, 2012). The locations of these faults are shown in Figure 5 and Figure S2 in Supporting Information S1.

direction (Figure 5 and Figure S5 in Supporting Information S1). Finally, further to the west (N13.40°–13.45°, E40.81°–40.85°), ~NS alignments of vents highlight another area of intense volcanic activity. Here, lavas are observed to have flowed eastward, forming the basaltic host rock where systems of young faults and fractures develop (Figure 5a).

Beyond the areas of focused magmatic activity, a central fault system at the Afrera Plain (Figure 5a) displays dominant tectonic features. By simply distinguishing between E-NE-dipping and W-SW-dipping faults, the weighted rose diagrams show two main structural trends in the area (Figures 5a and 5c–5e). The first trend is represented by the E-NE-dipping faults which have an average strike of N163°E ± 10°E, similar to that shown by the magmatic features elsewhere in the area. These faults are well developed, with maximum lengths and throws of ~4 km and 20 m, respectively (Figure 5c). Among them, the longest faults strike ~NS, some of which were responsible for the M_w 5 earthquakes that occurred at Afrera Plain (La Rosa et al., 2019, 2021). The ~NS-striking faults are observed to either develop as individual segments or form part of a more complex network. In particular, between N13.41° and N13.46°, left-stepping, NS-striking faults interact, creating a ~4-km-long, 2-km-wide, pull-apart basin with an architecture compatible to a left-lateral trans-tensional kinematics (Figure 5a; Figures S2 and S6 in Supporting Information S1; Dooley & Schreurs, 2012). Here, the internal S-shaped faults result from the growth of fractures and short fault segments that flip the dip-direction as they propagate to link (Figure 5a).

The second trend is represented by the W-SW-dipping faults which show an average strike of N153°E ± 4°E (Figure 5d). Although higher in number, such faults are shorter, with a maximum length of ~2 km. Moreover, ~60% of the fault population consists of short segments forming within the pull-apart basin (Figure S6 in Supporting Information S1). In other cases, such faults are arranged in conjugate systems with E-NE-dipping faults.

The two structural trends can be also recognized in the rose-diagram of faults without clear dip, likely due to the presence of both W-SW- and E-NE-dipping faults in this feature class (Figure 5e). In the Afrera Plain, the 50% of the faults without a clear dip have been mapped to the west in an area at the interaction with the Erta Ale segment (N13.43°–13.50°, E40.76°–40.80°; Figure 5). Here, the faults are arranged in a conjugate system with monoclines and shallow splays resulting from ruptures at depth that highlight structures with maximum lengths of ~4 km.

We analyzed patterns of fractures and splays along individual fault segments to determine their sense of slip (Figure 7). The analysis revealed the presence of Riedel structures that usually form above buried faults with a strike-slip component (e.g., Dooley & Schreurs, 2012). In detail, the ~NS-striking faults developed systems of overlapping left-lateral R shears, right-stepped by synthetic P shears with the same kinematics. Such a setting indicates the presence of a fault having a strike-slip left-lateral component (Figures 7a–7c; Figures S2 and S7 in Supporting Information S1). We also observed horsetail-type fractures at the fault tips which are compatible with the same kinematics (Figure S7 in Supporting Information S1). Riedel structures are also observed along NW-striking faults but indicating an opposite sense of slip, namely right lateral (Figures 7d–7f; Figures S2 and S8 in Supporting Information S1). In detail, overlapping R shears with right-lateral slip are left-stepped by synthetic P shears. In some cases, restraining bends at the tips of the R shears also form clear push-up structures elongated in the same direction of the buried fault (Figure 7). Some R shear is also characterized by a normal dip-slip component (Figures S2

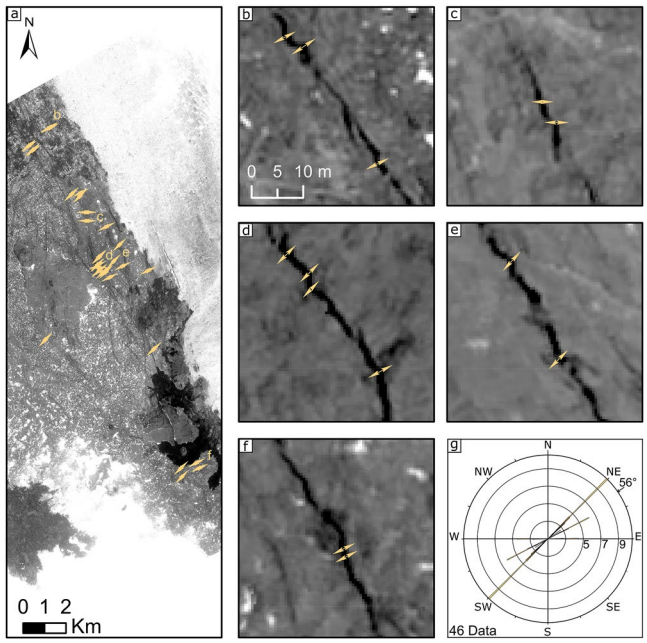

Figure 8. Fracture opening directions (orange arrows) measured at the main central fault system of Afrera Plain. (a) Map view showing the distribution of observation. (b–f) Close-up on the fracture measurements (the scale is reported in b). (g) Rose diagrams showing the distribution of opening directions. The binning is 1°. Note that the average value is N56°E, yet most measurements indicate a N45°E direction.

and S9 in Supporting Information S1), as predicted to form in trans-tensional settings by analog models (Dooley & Schreurs, 2012). Figure 7 and Figure S9 in Supporting Information S1 clearly show how ~NS- and NW-striking faults represent a conjugate setting.

At the main central fault system of the Afrera Plain, we also made 46 measurements of opening direction along fractures systems. From north to south, the fractures open with a direction ranging between N45°E and N90°E (Figure 8). Fractures opening in a similar direction do not cluster in specific areas, yet the measured values are randomly distributed across the whole fault systems. Overall, the fractures open with an average direction of N56°E and with the majority showing a N45°E direction (Figure 8). Furthermore, the fractures open orthogonal to their direction (pure extension) but in few cases we also observed an oblique opening indicating a shear component. The measured opening directions fit well the extension directions calculated from the InSAR models of both coseismic and time-progressive displacements by La Rosa et al. (2019, 2021) (Table S1). Additionally, our measurements are compatible with both the left-lateral slip observed at the ~NS-striking faults and the right-lateral slip along the NW-striking faults.

5. Discussion

In this study, we used a high-resolution Pléiades-1 data set to carry out a detailed mapping and structural analysis of tectonic and magmatic features at the Afrera Plain linkage zone as well as at the southern tip of the Erta Ale segment and the northern tip of the Tat Ali segment. Measurements of main tectonic and magmatic trends, along with measurements of fractures opening directions, provided new insights on the fault geometry, kinematics, and the relationships between tectonics and magmatism in a linkage zone between two magmatic segments.

The majority of features mapped at the southern tip of the Erta Ale segment are magmatic with evidences of recent-most activity observed in the axial zone (Figure 3). Eruptive fissures and dike-related narrow grabens are the expression of this magmatism indicating that diking is important in accommodating extension in the area. These results are in agreement with the general models of mature rift systems where extension is mainly accommodated along axial magmatic segments through magmatic activity and associated minor faulting (e.g., Buck, 2006; Hayward & Ebinger, 1996; Keir et al., 2009; Rowland et al., 2007). The narrow zone of magmatic activity is bounded on both sides by normal faults that shape the typical axial graben morphology observed elsewhere at symmetric spreading centers (e.g., Ebinger et al., 2010; Rowland et al., 2007). In topographically flat areas, dikes have been demonstrated to be emplaced orthogonally to the extension direction (e.g., Acocella & Neri, 2009; Nakamura, 1977; Rubin & Pollard, 1988). Accordingly, being the surface expression of dike emplacement, the orientation of the magmatic features can be used to retrieve the direction of extension at the southern tip of the Erta Ale segment. In particular, considering the N157°E ± 3°E direction measured for the eruptive fissures (Figures 3f–3h), the extension is N67°E ± 3°E (Figures 9a and 9b). This value is consistent with the N65°E-oriented plate extension observed by GPS measurements (Viltres et al., 2020) and also consistent with that derived by inversion of regional focal mechanism data (Zwaan et al., 2020).

In the area covered by Pléiades-1, the northern tip of the Tat Ali segment is characterized by dominant tectonic features with systems of SW- and NE-dipping normal faults having a very homogenous N147°E ± 3°E trend (Figures 4 and 9). The same trend is shown by the eruptive fissures mapped in both the Pléiades-1 and the ancillary low-resolution data sets. This trend is rotated 10° counterclockwise with respect to that measured at the EA segment, suggesting a different direction of extension in northern TA (Figure 9). Using the same approach adopted for the EA, we can infer an extension in northern Tat Ali oriented N57°E ± 3°E (Figure 9d). Clearly, this direction is orthogonal to tectonic features as well, suggesting they accommodate a pure normal dip-slip.

10.1029/2021TC007115

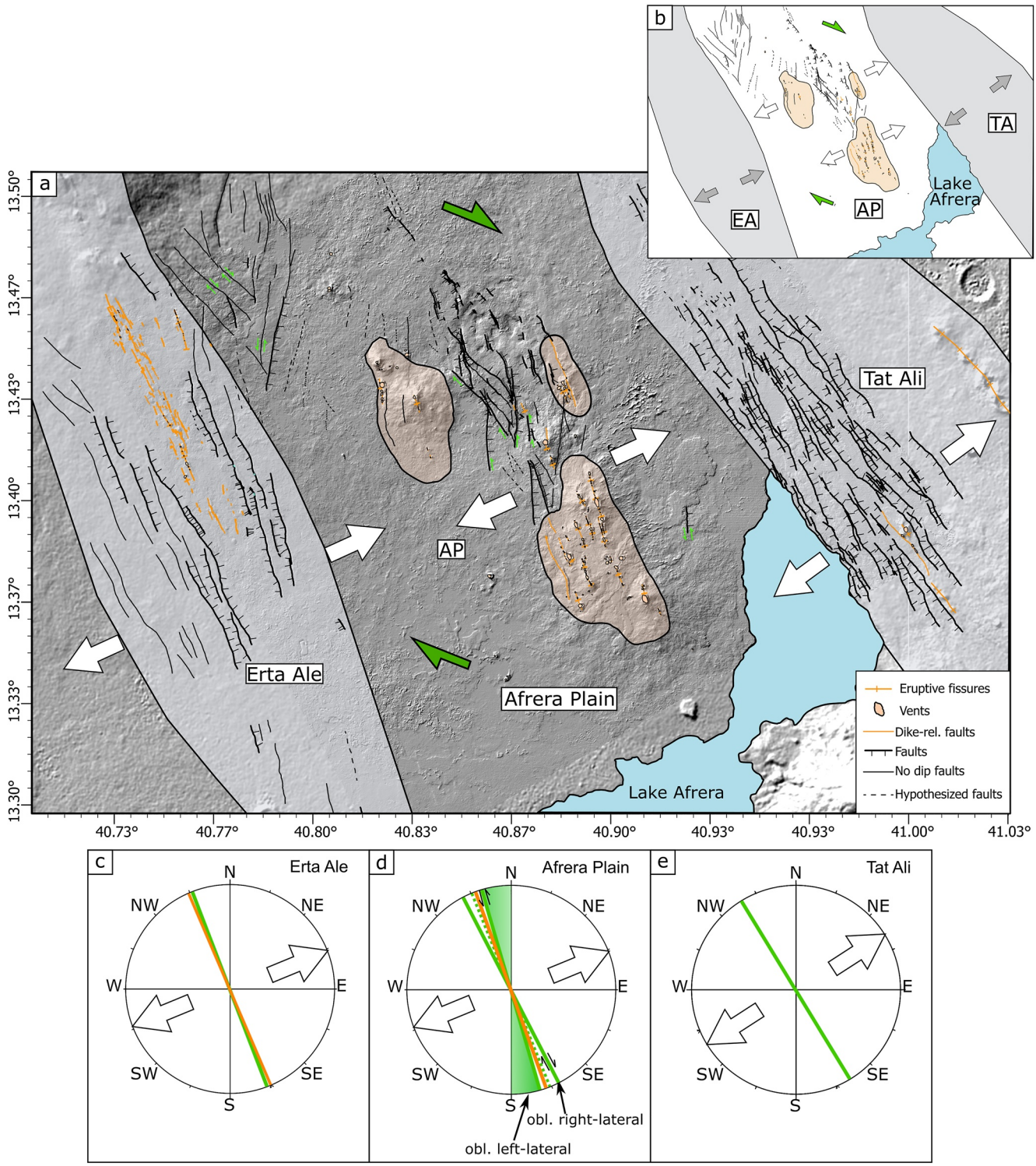

Figure 9. (a, b) Updated structural map and kinematic model of the Afrera Plain reporting the faults geometry and kinematics (dark green arrows) as also the main extension directions retrieved in this study. The fractures are not reported for an easy reading of the figure. The gray polygons are the main magmatic segments, while the orange ones represent the areas of magmatic activity in the Afrera Plain. The dark green arrows indicate the right-lateral shear motions. (c–e) Simplified sketches showing the directions of extension (white arrows) with respect to the average magmatic (orange thick lines) and tectonic trends (green thick lines). The shadowed green area in (c) represents the strike variability observed in the main oblique left-lateral fault system. The dashed green line is the bisector of the angle formed by the average strikes of the two fault families in the Afrera Plain.

The structural mapping at the Afrera Plain highlighted three main zones of magmatic activity at the center of the plain (Figure 5a). Here, eruptive fissures and dike-related faults have the same trend as those at the Erta Ale segment indicating the same extensional regime. Dark basaltic lava flows suggest that the recent-most fissural eruptions occurred in the south-central portion of Afrera Plain. These recent eruptive fissures are hosted within a half-graben controlled by east-dipping normal faults. An interplay between faulting at the flanks and magmatism at the center of the half-graben is evident where vents form on both sides of the walls. This is also supported by the observation of the fault cutting the older lavas but acting as a barrier for the recent-most ones (Figure 6a). In some cases, the recent lavas are also locally fractured above the scarp, likely indicating partial reactivation of the fault after their emplacement. In the Afrera Plain, where evidence of dike emplacement exists, the morphology of dike-related faults is characterized by monocline structures indicating a fault nucleation above the intruding dike and an upward propagation of the rupture (Figures 5b and 6; e.g., Holland et al., 2006).

An important result of this study is the retrieval of the geometry and kinematics of tectonic features in the Afrera Plain (Figure 9). We observed a conjugate system of N163°E ± 10°E striking, left-lateral oblique faults and N153°E ± 4°E striking, right-lateral oblique faults. Among the tectonic features, the former fault family also shows major ∼NS-striking faults and previous InSAR studies indicate that they currently accommodate most of the displacement in the area through oblique left-lateral slip (La Rosa et al., 2019, 2021). The detailed analysis of kinematic indicators also revealed the presence of horse-tail-type fractures and Riedel shears along NS-striking faults compatible with a left-lateral slip component that confirm the previous InSAR observations. In the Afrera Plain, low-magnitude earthquakes with focal mechanisms indicating that oblique right-lateral slips were also observed during 2011–2013 (Illsley-Kemp et al., 2018). Riedel shears at the surface confirm that such structures represent a conjugate fault population and have oblique right-lateral kinematics (Figure 7; Figures S8 and S9 in Supporting Information S1) in agreement with the focal mechanisms provided by Illsley-Kemp et al. (2018).

We observed a similar setting of conjugate faults further to the NW, at the interaction between the Erta Ale segment and the Afrera Plain (Figure 7). Here, some faults display clear throws and dip directions compatible with a normal component yet we also identified Riedel shears with the opposite sense of motion, similar to those characterizing the conjugate faults at the center of the Afrera Plain (Figure 5a; Figures S8 and S9 in Supporting Information S1). While the fault pattern is fairly complex, the kinematics and orientations of the conjugate faults can be interpreted as broadly consistent with the same ∼N65°E horizontal extension recorded in the magmatic features at the Erta Ale segment and the Afrera Plain (Figure 9). For example, assuming the N163°E ± 10°E striking left-lateral oblique faults and N153°E ± 4°E striking right-lateral oblique faults as a conjugate pair, yields ∼N68°E extension. The measurements of fractures opening directions collected across the whole main central fault system scatter around an average N56°E direction. Additionally, previous InSAR models of fault displacements show that the major faults at the Afrera Plain are characterized by an extension direction that varies between ∼N46°E and ∼N68°E (La Rosa et al., 2019, 2021).

The various structural and geodetic indicators, therefore, show extension in the Afrera linkage zone in the range of ∼N46°E–N68°E, a scatter that can be explained by the natural variability of fault strikes and slip sense due to factors such as rock anisotropy, and the local stress deflections and fault block rotations common in linkage zones (e.g., Corti et al., 2003; Muirhead et al., 2015). An interpretation that the dikes and faults form in the same strain field implies that they can be coeval, with dikes accommodating extension and the oblique slip faults accommodating extension and the shear strain. The tectonic interpretation and scatter of structurally recorded extension directions would be similar to other studies made across the East African Rift by Muirhead et al. (2015) and in Iceland by Tentler (2005) where dikes and faults orientations have been shown to jointly respond to the regional strain fields but also to their local perturbations at rift linkage zone.

An alternative scenario would imply the dikes and faults as being noncoeval. In this case, the dikes would have formed earlier compared to faults, which have then progressively accommodated the linkage between the Erta Ale and the Tat Ali segments with counterclockwise rotations, producing the wide range of interpreted extension directions that are biased in a counterclockwise sense. In literature, analog and numerical experiments, as well as field surveys, have shown that rotations of strain field can occur as a result of the mechanical interactions between adjacent magmatic segments (e.g., Bubeck et al., 2017; Glerum et al., 2020; Molnar et al., 2017; Morley, 2010; Muirhead et al., 2015; Neuharth et al., 2021; Rowland & Sibson, 2001; Zwaan & Schreurs, 2020). Similar block rotations have also been suggested by Muluneh et al. (2013) to occur further south in Afar, at the interaction between the Dabbahu–Manda-Harraro and Tat Ali segments. In the Reykjanes Peninsula oblique rift (Iceland),

intrusions and fissural eruption also strikes differently to faults and may occur at different times (e.g., Clifton & Schlische, 2003; Einarsson, 2008). Fully testing an hypothesis of progressive strain rotation through time would require combined age determination of the fault cut lava flows, combined with paleomagnetic measurements of rock rotations.

In previous studies, the variability in the extension direction at the Afrera Plain has been interpreted as resulting from a counterclockwise rotation of the strain field in the linkage zone due to interaction between the Erta Ale and Tat Ali segments (La Rosa et al., 2019). However, our new measurements of the orientation of magmatic features, along with the potential that the structurally interpreted extension simply reflects natural variability, make an interpretation of counterclockwise rotation of the strain field less certain. However, our results do show that both diking and faulting could occur in the Afrera Plain, with intermittent diking accommodating pure extension and conjugate oblique faults accommodating both extension and the shear strain resulting from the linkage between the Erta Ale and Tat Ali segments. This interpretation explains well our observations in the Afrera Plain and support the idea that magma is important in controlling plate spreading not only at the rift segments but also within the rift linkage zones.

6. Conclusion

A detailed mapping of the Afrera Plain from Pléiades-1 data allowed us to get a new picture of its structural architecture, shedding light on the fault geometry and kinematics, and also on the relationship between magmatism and tectonics at this linkage zone. Our observations expand on previous studies on the area (La Rosa et al., 2019, 2021) and the main results of our study can be summarized as follows.

1. A structural architecture made by conjugate oblique faults characterize both the center and the tips of the linkage zone. The analysis of surface structures allowed us to interpret the fault kinematics where Afrera Plain meets the Erta Ale segment and identify the faults responsible for right-lateral motions previously inferred just by seismicity. All the kinematic indicators in this study also confirm previous geodetic and seismic observations on the Afrera Plain, supporting the model of right-lateral linkage zone proposed for the area.
2. New measurements of magmatic features at the Afrera Plain indicate that they accommodate an extension oriented ~N65°E similar to the Erta Ale segment. Furthermore, the horizontal extension from new measurements of fracture opening direction and the conjugate setting of oblique faults across the whole Afrera Plain show scattering in the direction between N46°E and N68°E. Spatial relationships between lavas and faults also suggest that diking and faulting likely coexist in the area and both should respond to a similar strain field. The scatter of the extension could be thus related to local and intrinsic complexities of the linkage zone.
3. Intermittent dike intrusions and long-term oblique faulting occur at the Afrera Plain, with dikes accommodating pure extension, and oblique slip faults accommodating extension and the shear resulting from the linkage of Erta Ale and Tat Ali segments.

Data Availability Statement

The three high-resolution DEMs (Data Set S1) are publicly available and can be downloaded from the OSF Repository (La Rosa et al., 2022): https://doi.org/10.17605/OSF.IO/KXM8A.

Acknowledgments
This study is supported by the Ministero Università e Ricerca (MiUR) through PRIN grant 2017P9AT72. D. Keir acknowledges NERC grant NE/L013932/1. Pléiades-1 tri-stereo data have been provided by Airbus Defence and Space Intelligence under the ICR_FC_278100 - CEOS Volcano Demonstrator project. Shuttle Radar Topography Mission Digital Elevation Models (SRTM-DEM) can be downloaded from the U.S. Geological Survey Earth Explorer web service (https://earthexplorer.usgs.gov). Open Access Funding provided by Universita degli Studi di Pisa within the CRUI-CARE Agreement.

References

Acocella, V. (2006). Regional and local tectonics at Erta Ale caldera, Afar (Ethiopia). *Journal of Structural Geology*, *28*, 1808–1820. https://doi.org/10.1016/j.jsg.2006.06.014

Acocella, V. (2010). Coupling volcanism and tectonics along divergent plate boundaries: Collapsed rifts from Central Afar, Ethiopia. *GSA Bulletin*, *122*(9–10), 1717–1728. https://doi.org/10.1130/B30105.1

Acocella, V., Gudmundsson, A., & Funiciello, R. (2000). Interaction and linkage of extension fractures and normal faults: Examples from the rift zone of Iceland. *Journal of Structural Geology*, *22*, 1233–1246. https://doi.org/10.1016/S0191-8141(00)00031-6

Acocella, V., & Korme, T. (2002). Holocene extension direction along the Main Ethiopian Rift, East Africa. *Terra Nova*, *14*(3), 191–197. https://doi.org/10.1046/j.1365-3121.2002.00403.x

Acocella, V., & Neri, M. (2009). Dike propagation in volcanic edifices: Overview and possible developments. *Tectonophysics*, *471*(1–2), 67–77. https://doi.org/10.1016/j.tecto.2008.10.002

Barberi, F., Borsi, S., Ferrara, G., Marinelli, G., Santacroce, R., Tazieff, H., & Varet, J. (1972). Evolution of the Danakil Depression (Afar, Ethiopia) in light of radiometric age determinations. *The Journal of Geology*, *80*(6), 720–729. https://doi.org/10.1086/627797

Barberi, F., & Varet, J. (1970). The Erta Ale volcanic range (Danakil Depression, Northern Afar, Ethiopia). *Bulletin Volcanologique*, *34*(4), 848–917. https://doi.org/10.1007/BF02596805

Barberi, F., & Varet, J. (1972). *Geological map of the Erta Ale volcanic range (Danakil Depression, Ethiopia), approximate scale 1:100.000*. CNR-CNRS, Geotechnip.

Barberi, F., & Varet, J. (1977). Volcanism of Afar: Small-scale plate tectonics implications. *The Geological Society of America Bulletin*, *88*(70904), 1251–1266. https://doi.org/10.1130/0016-7606(1977)88<1251:VOASPT>2.0.CO;2

Barnie, T. D., Oppenheimer, C., & Pagli, C. (2016). Does the lava lake of Erta 'Ale volcano respond to regional magmatic and tectonic events? An investigation using Earth Observation data. *Geological Society, London, Special Publications*, *420*(1), 181–208. https://doi.org/10.1144/SP420.15

Battaglia, M., Pagli, C., & Meuti, S. (2021). The 2008–2010 subsidence of Dallol volcano on the spreading Erta Ale Ridge: InSAR observations and source models. *Remote Sensing*, *13*(10), 1–14. https://doi.org/10.3390/rs13101991

Beyene, A., & Abdelsalam, M. G. (2005). Tectonics of the Afar depression: A review and synthesis. *Journal of African Earth Sciences*, *41*(1–2), 41–59. https://doi.org/10.1016/j.jafrearsci.2005.03.003

Bonatti, E., Gasperini, E., Vigliotti, L., Lupi, L., Vaselli, O., Polonia, A., & Gasperini, L. (2017). Lake Afrera, a structural depression in the Northern Afar Rift (Red Sea). *Heliyon*, *3*(5), e00301. https://doi.org/10.1016/j.heliyon.2017.e00301

Brune, S., Corti, G., & Ranalli, G. (2017). Controls of inherited lithospheric heterogeneity on rift linkage: Numerical and analog models of interaction between the Kenyan and Ethiopian rifts across the Turkana depression. *Tectonics*, *36*, 1767–1786. https://doi.org/10.1002/2017TC004739

Bubeck, A., Walker, R. J., Imber, J., Holdsworth, R. E., Macleod, C. J., & Holwell, D. A. (2017). Extension parallel to the rift zone during segmented fault growth: Application to the evolution of the NE Atlantic. *Solid Earth*, *8*, 1161–1180. https://doi.org/10.5194/se-8-1161-2017

Bubeck, A., Walker, R. J., Imber, J., & MacLeod, C. J. (2018). Normal fault growth in layered basaltic rocks: The role of strain rate in fault evolution. *Journal of Structural Geology*, *115*(February), 103–120. https://doi.org/10.1016/j.jsg.2018.07.017

Buck, W. R. (2006). The role of magma in the development of the Afro-Arabian Rift System. *Geological Society, London, Special Publications*, *259*, 43–54. https://doi.org/10.1144/GSL.SP.2006.259.01.05

Calvari, S. (2019). Understanding basaltic lava flow morphologies and structures for hazard assessment. *Annals of Geophysics*, *62*(2 Special Issue), 1–17. https://doi.org/10.4401/ag-8048

Cashman, K. V., Soule, S. A., Mackey, B. H., Deligne, N. I., Deardorff, N. D., & Dietterich, H. R. (2013). How lava flows: New insights from applications of lidar technologies to lava flow studies. *Geosphere*, *9*(6), 1664–1680. https://doi.org/10.1130/GES00706.1

Clifton, A. E., & Schlische, R. W. (2003). Fracture populations on the Reykjanes Peninsula, Iceland: Comparison with experimental clay models of oblique rifting. *Journal of Geophysical Research*, *108*(B2), 2074. https://doi.org/10.1029/2001JB000635

Corti, G. (2012). Evolution and characteristics of continental rifting: Analog modeling-inspired view and comparison with examples from the East African Rift System. *Tectonophysics*, *522–523*(1), 1–33. https://doi.org/10.1016/j.tecto.2011.06.010

Corti, G., Bonini, M., Conticelli, S., Innocenti, F., Manetti, P., & Sokoutis, D. (2003). Analogue modelling of continental extension: A review focused on the relations between the patterns of deformation and the presence of magma. *Earth-Science Reviews*, *63*(3–4), 169–247. https://doi.org/10.1016/s0012-8252(03)00035-7

Corti, G., Bonini, M., Mazzarini, F., Boccaletti, M., Innocenti, F., Manetti, P., et al. (2002). Magma-induced strain localization in centrifuge models of transfer zones. *Tectonophysics*, *348*, 205–218. https://doi.org/10.1016/s0040-1951(02)00063-x

Corti, G., Bonini, M., Sokoutis, D., Innocenti, F., Manetti, P., Cloetingh, S., & Mulugeta, G. (2004). Continental rift architecture and patterns of magma migration: A dynamic analysis based on centrifuge models. *Tectonics*, *23*, TC2012. https://doi.org/10.1029/2003TC001561

Dooley, T. P., & Schreurs, G. (2012). Analogue modelling of intraplate strike-slip tectonics: A review and new experimental results. *Tectonophysics*, *574*(575), 1–71. https://doi.org/10.1016/j.tecto.2012.05.030

Doubre, C., Déprez, A., Masson, F., Socquet, A., Lewi, E., Grandin, R., et al. (2017). Current deformation in Central Afar and triple junction kinematics deduced from GPS and InSAR measurements. *Geophysical Journal International*, *208*(2), 936–953. https://doi.org/10.1093/gji/ggw434

Eagles, G., Gloaguen, R., & Ebinger, C. (2002). Kinematics of the Danakil microplate. *Earth and Planetary Science Letters*, *203*(2), 607–620. https://doi.org/10.1016/S0012-821X(02)00916-0

Ebinger, C. (1989). Geometric and kinematic development of border faults and accommodation zones, Kivu–Rusizi Rift, Africa. *Tectonics*, *8*(1), 117–133. https://doi.org/10.1029/TC008i001p00117

Ebinger, C., Ayele, A., Keir, D., Rowland, J., Yirgu, G., Wright, T., et al. (2010). Length and timescales of rift faulting and magma intrusion: The Afar rifting cycle from 2005 to present. *Annual Review of Earth and Planetary Sciences*, *38*(February), 439–466. https://doi.org/10.1146/annurev-earth-040809-152333

Ebinger, C. J., Deino, A. L., Drake, R. E., & Tesha, A. L. (1989). Chronology of volcanism and rift basin propagation: Rungwe Volcanic Province, East Africa. *Journal of Geophysical Research*, *94*(B11), 785–803. https://doi.org/10.1029/JB094iB11p15785

Einarsson, P. (2008). Plate boundaries, rift and transforms in Iceland. *Jökull Journal*, *58*, 35–58.

Einarsson, P., & Brandsdóttir, B. (1980). Seismological evidence for Lateral magma intrusion during the July 1978 deflation of the Krafla volcano in NE-Iceland. *Journal of Geophysics*, *47*, 160–165. https://doi.org/10.2172/890964

Farr, T. G., Rosen, P., Caro, E., Crippen, R., Duren, R., Hensley, S., et al. (2007). The Shuttle Radar Topography Mission. *Reviews of Geophysics*, *45*, RG2004. https://doi.org/10.1029/2005RG000183

Faulds, J. E., & Varga, R. J. (1998). The role of accommodation zones and transfer zones in the regional segmentation of extended terranes. In *Geological Society of America Special Paper 323*. https://doi.org/10.1130/0-8137-2323-X.1

Glerum, A., Brune, S., Stamps, D. S., & Strecker, M. R. (2020). Victoria continental microplate dynamics controlled by the lithospheric strength distribution of the East African Rift. *Nature Communications*, *11*, 2881. https://doi.org/10.1038/s41467-020-16176-x

Gleyzes, M. A., Perret, L., & Kubik, P. (2012). Pleiades system architecture and main performances. In *XXII ISPRS Congress, 25 August to 01 September 2012, Melbourne, Australia* (pp. 537–542). https://doi.org/10.5194/isprsarchives-XXXIX-B1-537-2012

Grandin, R., Socquet, A., Jacques, E., Mazzoni, N., Chabalier, J. B. D., & King, G. C. P. (2010). Sequence of rifting in Afar, Manda-Hararo rift, Ethiopia, 2005–2009: Time–space evolution and interactions between dikes from interferometric synthetic aperture radar and static stress change modeling. *Journal of Geophysical Research*, *115*, B10413. https://doi.org/10.1029/2009JB000815

Gudmundsson, A. (2003). *Surface stresses associated with arrested dykes in rift zones* (pp. 606–619). https://doi.org/10.1007/s00445-003-0289-7

Hayward, N. J., & Ebinger, C. J. (1996). Variations in the along-axis segmentation of the Afar. *Tectonics*, *15*(2), 1–14. https://doi.org/10.1029/95TC02292

Holland, M., Urai, J. L., & Martel, S. (2006). The internal structure of fault zones in basaltic sequences. *Earth and Planetary Science Letters*, *248*(1–2), 301–315. https://doi.org/10.1016/j.epsl.2006.05.035

Illsley-Kemp, F., Bull, J. M., Keir, D., Gerya, T., Pagli, C., Gernon, T., et al. (2018). Initiation of a proto-transform fault prior to seafloor spreading. *Geochemistry, Geophysics, Geosystems*, *19*, 4744–4756. https://doi.org/10.1029/2018GC007947

Keir, D., Hamling, I. J., Ayele, A., Calais, E., Ebinger, C., Wright, T. J., et al. (2009). Evidence for focused magmatic accretion at segment centers from lateral dike injections captured beneath the Red Sea rift in Afar. *Geology*, *37*(1), 59–62. https://doi.org/10.1130/G25147A.1

Kim, Y. S., Peacock, D. C. P., & Sanderson, D. J. (2004). Fault damage zones. *Journal of Structural Geology*, *26*(3), 503–517. https://doi.org/10.1016/j.jsg.2003.08.002

Koopmann, H., Brune, S., Franke, D., & Breuer, S. (2014). Linking rift propagation barriers to excess magmatism at volcanic rifted margins. *Geology*, *42*(12), 1071–1074. https://doi.org/10.1130/G36085.1

La Rosa, A., Pagli, C., Hurman, G., & Keir, D. (2022). *High-resolution DEMs of Afrera Plain (Ethiopia) from Pléiades-1 tri-stereo imagery*. https://doi.org/10.17605/OSF.IO/KXM8A

La Rosa, A., Pagli, C., Keir, D., Sani, F., Corti, G., Wang, H., & Possee, D. (2019). Observing oblique slip during rift linkage in Northern Afar. *Geophysical Research Letters*, *46*, 10782–10790. https://doi.org/10.1029/2019GL084801

La Rosa, A., Pagli, C., Wang, H., Doubre, C., Leroy, S., Sani, F., et al. (2021). Plate-boundary kinematics of the Afrera linkage zone (Afar) from InSAR and seismicity. *Journal of Geophysical Research: Solid Earth*, *126*, e2020JB021387. https://doi.org/10.1029/2020JB021387

Le Pourhiet, L., May, D. A., Huille, L., Watremez, L., & Leroy, S. (2017). A genetic link between transform and hyper-extended margins. *Earth and Planetary Science Letters*, *465*, 184–192. https://doi.org/10.1016/j.epsl.2017.02.043

Manighetti, I., Tapponnier, P., Courtillot, V., Gallet, Y., Jacques, E., & Gillot, P. Y. (2001). Strain transfer between disconnected, propagating rifts in Afar. *Journal of Geophysical Research*, *106*(B7), 13613–13665. https://doi.org/10.1029/2000JB900454

Manighetti, I., Tapponnier, P., Gillot, P. Y., Jacques, E., Courtillot, V., Armijo, R., et al. (1998). Propagation of rifting along the Arabia–Somalia plate boundary: Into Afar. *Journal of Geophysical Research*, *103*(3), 4947–4974. https://doi.org/10.1029/97JB02758

McClusky, S., Reilinger, R., Ogubazghi, G., Amleson, A., Healeb, B., Vernant, P., et al. (2010). Kinematics of the southern Red Sea–Afar triple junction and implications for plate dynamics. *Geophysical Research Letters*, *37*, L05301. https://doi.org/10.1029/2009GL041127

Molnar, N. E., Cruden, A. R., & Betts, P. G. (2017). Interactions between propagating rotational rifts and linear rheological heterogeneities: Insights from three-dimensional laboratory experiments. *Tectonics*, *36*, 420–443. https://doi.org/10.1002/2016TC004447

Moore, C., Wright, T., Hooper, A., & Biggs, J. (2019). The 2017 eruption of Erta 'Ale volcano, Ethiopia: Insights into the shallow axial plumbing system of an incipient mid-ocean ridge. *Geochemistry, Geophysics, Geosystems*, *20*, 5727–5743. https://doi.org/10.1029/2019GC008692

Morley, C. K. (2010). Stress re-orientation along zones of weak fabrics in rifts: An explanation for pure extension in 'oblique' rift segments? *Earth and Planetary Science Letters*, *297*, 667–673. https://doi.org/10.1016/j.epsl.2010.07.022

Muirhead, J. D., Kattanhorn, S. A., & Le Corvec, N. (2015). Varying styles of magmatic strain accommodation across the East African Rift. *Geochemistry, Geophysics, Geosystems*, *16*, 2775–2795. https://doi.org/10.1002/2015GC005918

Muluneh, A. A., Kidane, T., Rowland, J., & Bachtadse, V. (2013). Tectonophysics counterclockwise block rotation linked to southward propagation and overlap of sub-aerial Red Sea Rift segments, Afar depression: Insight from paleomagnetism. *Tectonophysics*, *593*, 111–120. https://doi.org/10.1016/j.tecto.2013.02.030

Nakamura, K. (1977). Volcanoes as possible indicators of tectonic stress orientation—Principle and proposal. *Journal of Volcanology and Geothermal Research*, *2*(1), 1–16. https://doi.org/10.1016/0377-0273(77)90012-9

Neuharth, D., Brune, S., Glerum, A., Heine, C., & Welford, K. J. (2021). Formation of continental microplates through rift linkage : Numerical modeling and its application to the Flemish Cap and Sao Paulo plateau. *Geochemistry, Geophysics, Geosystems*, *22*, e2020GC009615. https://doi.org/10.1029/2020GC009615

Nobile, A., Pagli, C., Keir, D., Wright, T. J., Ayele, A., Ruch, J., & Acocella, V. (2012). Dike-fault interaction during the 2004 Dallol intrusion at the northern edge of the Erta Ale Ridge (Afar, Ethiopia). *Geophysical Research Letters*, *39*, L19305. https://doi.org/10.1029/2012GL053152

Pagli, C., Mazzarini, F., Keir, D., Rivalta, E., Rooney, T. O., Pisa, U., & Maria, V. S. (2015). Introduction: Anatomy of rifting: Tectonics and magmatism in continental rifts, oceanic spreading centers, and transforms. *Geosphere*, *11*(5), 1–6. https://doi.org/10.1130/GES01082.1

Pagli, C., Wright, T. J., Ebinger, C. J., Yun, S.-H., Cann, J. R., Ayele, A., & Barnie, T. (2012). Shallow axial magma chamber at the slow-spreading Erta Ale Ridge. *Nature Geoscience*, *5*(4), 284–288. https://doi.org/10.1038/ngeo1414

Pagli, C., Yun, S.-H., Ebinger, C., Keir, D., & Wang, H. (2019). Strike-slip tectonics during rift linkage. *Geology*, *47*(1), 31–34. https://doi.org/10.1130/g45345.1

Rowland, J. R., & Sibson, R. H. (2001). Extensional fault kinematics within the Taupo Volcanic Zone, New Zealand: Soft-linked segmentation of a continental rift system. *New Zealand Journal of Geology and Geophysics*, *44*, 271–283. https://doi.org/10.1080/00288306.2001.9514938

Rowland, J. V., Baker, E., Ebinger, C. J., Keir, D., Kidane, T., Biggs, J., et al. (2007). Fault growth at a nascent slow-spreading ridge: 2005 Dabbahu rifting episode, Afar. *Geophysical Journal International*, *171*(3), 1226–1246. https://doi.org/10.1111/j.1365-246X.2007.03584.x

Rubin, A. M., & Pollard, D. D. (1988). Dike-induced faulting in rift zones of Iceland and Afar. *Geology*, *16*(5), 413–417. https://doi.org/10.1130/0091-7613(1988)016<0413:DIFIRZ>2.3.CO;2

Schaegis, J., Rime, V., Kidane, T., Mosar, J., Atnafu, B., & Foubert, A. (2021). Novel bathymetry of lake Afdera reveals fault structures and volcano-tectonic features of an incipient transform zone. *Frontiers of Earth Science*, *9*(July), 1–13. https://doi.org/10.3389/feart.2021.706643

Sigmundsson, F., Hooper, A., Hreinsdóttir, S., Vogfjörd, K. S., Ófeigsson, B. G., Heimisson, E. R., et al. (2015). Segmented lateral dyke growth in a rifting event at Bárðarbunga volcanic system, Iceland. *Nature*, *517*, 191–195. https://doi.org/10.1038/nature14111

Tentler, T. (2005). Propagation of brittle failure triggered by magma in Iceland. *Tectonophysics*, *406*, 17–38. https://doi.org/10.1016/j.tecto.2005.05.016

Tibaldi, A., Bonali, F. L., Einarsson, P., Hjartardóttir, Á. R., & Pasquaré Mariotto, F. (2016). Partitioning of Holocene kinematics and interaction between the Theistareykir fissure swarm and the Husavik-Flatey Fault, North Iceland. *Journal of Structural Geology*, *83*, 134–155. https://doi.org/10.1016/j.jsg.2016.01.003

Tibaldi, A., Bonali, F. L., Pasquaré Mariotto, F., Corti, N., Russo, E., Einarsson, P., & Hjartardóttir, Á. R. (2020). Rifting kinematics produced by magmatic and tectonic stresses in the north volcanic zone of Iceland. *Frontiers of Earth Science*, *8*(June), 1–18. https://doi.org/10.3389/feart.2020.00174

Tortelli, G., Gioncada, A., Pagli, C., Rosi, M., Dosso, L. D., & Keir, D. (2021). Evidence of active magmatic rifting at the Ma'Alalta volcanic field (Afar, Ethiopia). *Bulletin of Volcanology*, *83*, 38. https://doi.org/10.1007/s00445-021-01461-4

Toutin, T., & Cheng, P. (2002). Comparison of automated digital elevation model extraction results using along-track ASTER and across track SPOT stereo images. *Optical Engineering*, *41*(9). https://doi.org/10.1117/1.1496111

Trippanera, D., Acocella, V., Ruch, J., & Abebe, B. (2015). Fault and graben growth along active magmatic divergent plate boundaries in Iceland and Ethiopia. *Tectonics*, *34*, 2318–2348. https://doi.org/10.1002/2015TC003991

Trippanera, D., Ruch, J., Acocella, V., & Rivalta, E. (2015). Experiments of dike-induced deformation: Insights on the long-term evolution of divergent plate boundaries. *Journal of Geophysical Research: Solid Earth*, *120*, 6913–6942. https://doi.org/10.1002/2014JB011850

Trippanera, D., Ruch, J., Passone, L., & Jónsson, S. (2019). Structural mapping of dike-induced faulting in Harrat Lunayyir (Saudi Arabia) by using high resolution drone imagery. *Frontiers of Earth Science*, *7*(July), 1–23. https://doi.org/10.3389/feart.2019.00168

Viltres, R., Jónsson, S., Ruch, J., Doubre, C., Reilinger, R., Floyd, M., & Ogubazghi, G. (2020). Kinematics and deformation of the southern Red Sea region from GPS observations. *Geophysical Journal International*, *221*(3), 2143–2154. https://doi.org/10.1093/gji/ggaa109

Watts, E. J., Gernon, T. M., Taylor, R. N., Keir, D., Siegburg, M., Jarman, J., et al. (2020). Evolution of the Alu-Dalafilla and Borale volcanoes, Afar, Ethiopia. *Journal of Volcanology and Geothermal Research*, *408*, 107094. https://doi.org/10.1016/j.jvolgeores.2020.107094

Wentworth, C. K. (1954). The physical behavior of basaltic lava flows. *The Journal of Geology*, *62*(5), 425–438. https://doi.org/10.1086/626190

Wilson, M. F. J., O'Connell, B., Brown, C., Guinan, J. C., & Grehan, A. J. (2007). Multiscale terrain analysis of multibeam bathymetry data for habitat mapping on the continental slope. *Marine Geodesy*, *30*(1–2), 3–35. https://doi.org/10.1080/01490410701295962

Wright, T. J., Sigmundsson, F., Pagli, C., Belachew, M., Hamling, I. J., Brandsdóttir, B., et al. (2012). Geophysical constraints on the dynamics of spreading centres from rifting episodes on land. *Nature Geoscience*, *5*(4), 242–250. https://doi.org/10.1038/ngeo1428

Xu, W., Rivalta, E., & Li, X. (2017). Magmatic architecture within a rift segment: Articulate axial magma storage at Erta Ale volcano, Ethiopia. *Earth and Planetary Science Letters*, *476*, 79–86. https://doi.org/10.1016/j.epsl.2017.07.051

Zwaan, F., Corti, G., Sani, F., Keir, D., Muluneh, A. A., Illsley-Kemp, F., & Papini, M. (2020). Structural analysis of the Western Afar Margin, East Africa: Evidence for multiphase rotational rifting. *Tectonics*, *39*, e2019TC006043. https://doi.org/10.1029/2019TC006043

Zwaan, F., & Schreurs, G. (2020). Rift segment interaction in orthogonal and rotational extension experiments: Implications for the large-scale development of rift systems. *Journal of Structural Geology*, *140*, 104119. https://doi.org/10.1016/j.jsg.2020.104119